Applied Catalysis B: Environmental 185 (2016) 371–377

Contents lists available at ScienceDirect

Applied Catalysis B: Environmental

journal homepage: www.elsevier.com/locate/apcatb

Catalytic activities of dissolved and Sch-immobilized Mo in H_2O_2 decomposition: Implications for phenol oxidation under acidic conditions

Lin-Dong Liu[a,b,c], Wei-Min Wang[d], Lu Liu[d], Bo Yu[e], Yu-Xin Zhang[f], Xiao-Qing Wu[a], Hong-Wei Zhang[d], Xu Han[g,*]

[a] Key Laboratory of Advanced Textile Composites, Ministry of Education, Tianjin Polytechnic University, Tianjin, PR China
[b] School of Textiles, Tianjin Polytechnic University, Tianjin, PR China
[c] State Key Laboratory of Separation Membranes and Membrane Processes, Tianjin Polytechnic University, Tianjin, PR China
[d] School of Environmental and Chemical Engineering, Tianjin Polytechnic University, Tianjin, PR China
[e] School of Chemical Engineering and Technology, Tianjin University, Tianjin, PR China
[f] College of Materials Science and Engineering, Chongqing University, Chongqing, PR China
[g] School of Environmental Science and Engineering, Tianjin University, Tianjin, PR China

ARTICLE INFO

Article history:
Received 6 October 2015
Received in revised form
14 November 2015
Accepted 6 December 2015
Available online 17 December 2015

Keywords:
Molybdate
Schwertmannite
H_2O_2
Singlet oxygen
Phenol
•OOH

ABSTRACT

Schwertmannite (Sch), a good geo-sorbent for immobilizing molybdate oxyanion in natural environment, has been used as an efficient Fenton-like catalyst in the remediation of organic pollutants. However, what's the influence of immobilized molybdate (Mo_{imm}) on the catalytic activity of Sch and what's the catalytic difference between Mo_{imm} and dissolved molybdate (Mo_{diss}) in H_2O_2 activation are still unknown. In this study, we first find a dual mechanism of Mo-Sch involved in phenol oxidation. At low Mo_{imm} loadings (0.01Mo-Sch and 0.05Mo-Sch), phenol oxidation is predominantly mediated by HO• radicals generated from dissolved Fe(III) or surface ≡Fe(III) on Sch, whereas at high loadings (1Mo-Sch and 10Mo-Sch), •OOH as well as $^1O_2$ generated from monomeric Mo complexes on Sch under acidic conditions also play important roles in phenol oxidation. Unlike Mo-Sch, Mo_{diss} forms dimeric $Mo_2O_3(O_2)_4^{2-}$ with H_2O_2 under acidic conditions, which can oxidize phenol directively or via •OOH radicals, generated from dissolved $Mo_2O_3(O_2)_4^{2-}$. The dimerization of Mo_{diss} with H_2O_2 inhibits $^1O_2$ generation. During the experiments, Mo_{diss} can also interfere with the chain reactions between dissolved Fe(III) and H_2O_2, accelerating H_2O_2 decomposition via an O_2 generation pathway, which significantly reduces the utilization efficiency of H_2O_2 in phenol oxidation.

1. Introduction

Hydrogen peroxide (H_2O_2) is a strong oxidant (E_0 = 0.87–1.80 V) that is extensively used for the oxidation of various organic pollutants. It can be decomposed via different pathways and generates various oxidative radicals such as hydroxyl radicals (HO•), superoxide radicals (•OOH/O_2^{-}•), singlet oxygen ($^1O_2$), or forms oxidative species with transitional metals such as TAML [1–3]. Among all these radicals, HO• radicals generated from Fenton or Fenton-like reactions can non-selectively degrade organic contaminants to smaller molecules or CO_2. Our recent study suggested that schwertmannite (Sch), an Fe(III)-oxyhydroxysulfate mineral, exhibited an excellent catalytic activity in the degradation of phenol by activating H_2O_2 via a HO• pathway [4]. Large quantities of HO• radicals generated from dissolved or immobilized Fe(III) on Sch can completely oxidize phenol in a short time under acidic conditions [4]. Recently, Duan et al. [5] also pointed out that HO• generated from the activation of H_2O_2 by Sch contributed to 92.5% removal of nitrobenzene within 30 min at pH 3.0.

Dissolved molybdate (Mo_{diss}) is an interesting oxyanion that can be transformed by H_2O_2 to various monomeric peroxomolybdates, such as $MoO_3(O_2)^{2-}$, $MoO_2(O_2)_2^{2-}$, $MoO(O_2)_3^{2-}$ and $Mo(O_2)_4^{2-}$ via Eq. (6) or a tetraperoxodimolybdate, $Mo_2O_3(O_2)_4^{2-}$ via Eq. (5) [6–8]. In the pH range of 2.5–5.0, $Mo_2O_3(O_2)_4^{2-}$ is a predominant Mo species and plays an important role in epoxidation of olefins and alcohols [6,7,9]. Under alkaline conditions, $MoO_3(O_2)^{2-}$, $MoO_2(O_2)_2^{2-}$, $MoO(O_2)_3^{2-}$ and $Mo(O_2)_4^{2-}$ are predominant species and can evolve $^1O_2$ (Eq. (1)) to effectively

* Corresponding author.
E-mail address: xuhan@tju.edu.cn (X. Han).

http://dx.doi.org/10.1016/j.apcatb.2015.12.010
0926-3373/

peroxidize organics [7,10,11]. Sels et al. [9,12] further pointed out that only monomeric Mo on layered double hydroxides (LDHs) could accelerate the generation rate of $^1O_2$ under alkaline conditions, and the amount of $^1O_2$ in Mo-LDHs system was only half of that generated in the Mo_{diss} system. However, what's the catalytic activity of Mo-LDHs under acidic conditions has not been investigated due to the easy dissolution of LDHs at low pHs.

$$2H_2O_2 \xrightarrow[\text{pH 9–12}]{MoO_4^{2-}} 2H_2O + {}^1O_2 \quad (1)$$

In natural environments, molybdate is always associated with Sch or other iron (oxyhydr) oxides in tailings and AMD from the molybdenite [13–16]. Yager et al. [13] found that Mo concentrations in soil on the Mount Moly, Silverton, Colorado, U.S. always ranged from 2 to 1700 mg g^{-1} soil, and X-ray diffraction (XRD) analysis confirmed the occurrence of Sch in the debris fans. In addition, Hayes et al. [14] noticed that molybdate precipitated as ferrimolybdite [$Fe_2(MoO_4)_3 \cdot 8H_2O$] or was adsorbed on ferrihydrite [MoO_4–$Fe(OH)_3$] during tailing preparation processes. Given the high specific surface area, Sch shows a high adsorption capacity to molybdate, with a maximal adsorption capacity of 115 mmol MoO_4^{2-} mol^{-1} Fe at pH 4.5 [17]. Similar ionic radius and charge of molybdate with SO_4^{2-} also facilitate it to exchange with the adsorbed or the structural SO_4^{2-} in Sch [17,18].

Owing to the close geochemical relationships between Mo and Sch, it is necessary to consider the influence of Mo on the catalytic activity of Sch in Fenton-like reactions. To the best of our knowledge, the presence of Mo on the catalytic activity of iron oxides during Fenton-like reactions has not been reported. In addition, mechanisms involved in H_2O_2 decomposition catalyzed by Sch immobilized Mo (Mo-Sch) and Mo_{diss} may be different under acidic conditions, given that HO• radicals generated from Sch may interfere with activation of H_2O_2 by Mo_{imm}. In this study, catalytic activity of Mo_{diss} and Mo-Sch in H_2O_2 activation under acidic conditions will be compared in the oxidation of phenol, a highly toxic contaminant which poses serious threats to human health and our environment [19,20]. Mechanisms of H_2O_2 activation involved in these processes will also be explored.

2. Experimental

2.1. Chemicals

All chemicals were of analytical grade or higher purity, and all solutions were prepared in deionized water. $Fe_2(SO_4)_3$ and *tert*-butanol were obtained from Tianjin Bodi Chemical Co. Ltd., $NaH_2AsO_4.7H_2O$ was purchased from Merck, and Na_2MoO_4, 38% HCl, 98% H_2SO_4, 30% H_2O_2, NaOH and phenol were purchased from Tianjin Bei Fang Chemical Co. Ltd.

2.2. Methodology

2.2.1. Preparation of Sch and Sch-Mo and phenol oxidation experiments

Freeze-dried Sch [$Fe_8O_8(OH)_{8-2x}(SO_4)_x$, $1 \le x \le 1.75$] was prepared according to the method described previously [4]. Sch-Mo was prepared by dispersing 0.15 g freeze-dried Sch in 100 mL deionized water for 2 h. A measured amount of concentrated molybdate stock was then added into the suspension, with a final working volume of 150 mL. pH was then adjusted to 3.0 by 1.0 M HCl or NaOH. Samples were then placed on a shaker at 150 rpm and 25 °C for 24 h to reach adsorption equilibrium. After that, Sch-Mo was centrifuged and re-dispersed in 100 mL deionized water with the pH of 3.0. Sch after the addition of 0.01–10 mM molybdate are named after 0.01Mo-Sch, 0.1Mo-Sch, 1Mo-Sch, etc. The suspension was subsequently mixed with a 50 mL phenol solution with the pH of 3.0. Oxidation of phenol was initiated with the addition of a measured amount of 30% H_2O_2. The experiments were carried out in dark to avoid possible photochemical reactions involved in oxidation processes. Initial concentrations of H_2O_2 and phenol were always controlled at 500 and 100 mg L^{-1}, respectively. The flasks were then placed on a shaker with a rotation speed of 150 rpm, and 4 mL sample was regularly taken out and centrifuged at 10,000 rpm for 5 min. Concentrations of H_2O_2, phenol, dissolved molybdate and Fe in the supernatant were then measured. All experiments were conducted in duplicate at 25 °C and the average values were recorded.

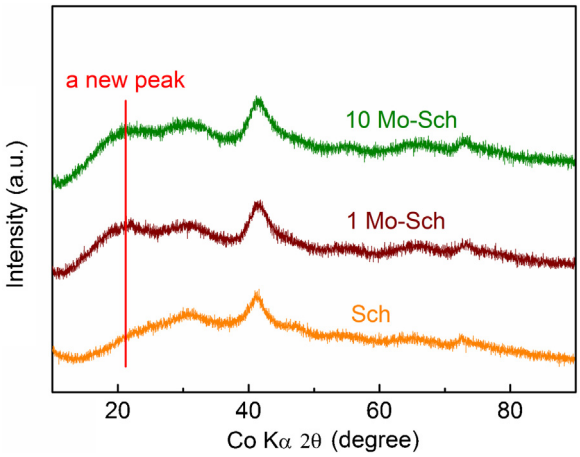

Fig. 1. XRD analysis of Sch Mo-Sch. Initial concentration of Sch was 1 g L^{-1} with a working volume of 150 mL after 24 h.

2.2.2. Analytical methods

The 4-aminoantipyrine method was used for the measurement of phenol concentration [21], and the detection limit was 0.1 mg L^{-1} as determined in our previous study [4]. Concentration of H_2O_2 was determined by a titanium sulfate method [22]. Inductively Coupled Plasma (ICP, Varian 715S) was also employed to determine dissolved Fe and molybdate.

The morphology of Sch and Sch-Mo was examined by a high-resolution TEM (JEM-2100F, JEOL). The crystalline structure of the synthetic Sch and Mo-Sch were characterized by XRD (D/Max-2500, Rigaku) with a Co X-ray source (λ = 1.7902 Å). Samples were scanned from 2θ = 10–90° with a 2θ = 0.02° step-size. EPR spin trapping analysis was performed on a Bruker EMX 10/12 spectrometer with 5,5-dimethyl-1-pyrroline *N*-oxide (DMPO) as a spin-trapping agent. Surface properties of Mo-Sch were characterized with a Thermo Nicolet Nexus FTIR spectrometer via a KBr pressed disk.

3. Results and discussion

3.1. Characterization of Sch and Mo-Sch

Characteristic peaks of the synthesized Sch agree well with the standard Sch card (Fig. 1, PDF 47-1775), and the Fe oxyhydroxide displays a needle-like morphology with a diameter of ca. 100 nm (Fig. 2a). ICP analysis indicates a formula of $Fe_8O_8(OH)_{4.5}(SO_4)_{1.75}$ of this Sch. FTIR spectrum exhibits characteristic —OH deformation (δ_{OH} at 860 and 712 cm^{-1}) and stretching (ν_{OH} at 3300 cm^{-1}) vibrations of Sch (Fig. 3). The typical S—O stretching (ν_{SO}) modes consist of a broad ν_3 band at 1120, 1190 and 1030 cm^{-1}, a ν_1 fundamental of the symmetric SO_4^{2-} stretch at 985 cm^{-1}, and a ν_4 bending band at 610 cm^{-1} (Fig. 3) [23].

XRD analysis of Sch-Mo shows a more intense peak at 41.80° in 1Mo-Sch and 10Mo-Sch, implying that high concentrations of Mo_{imm} enhance the crystalline degree of Sch (Fig. 1). Previous stud-

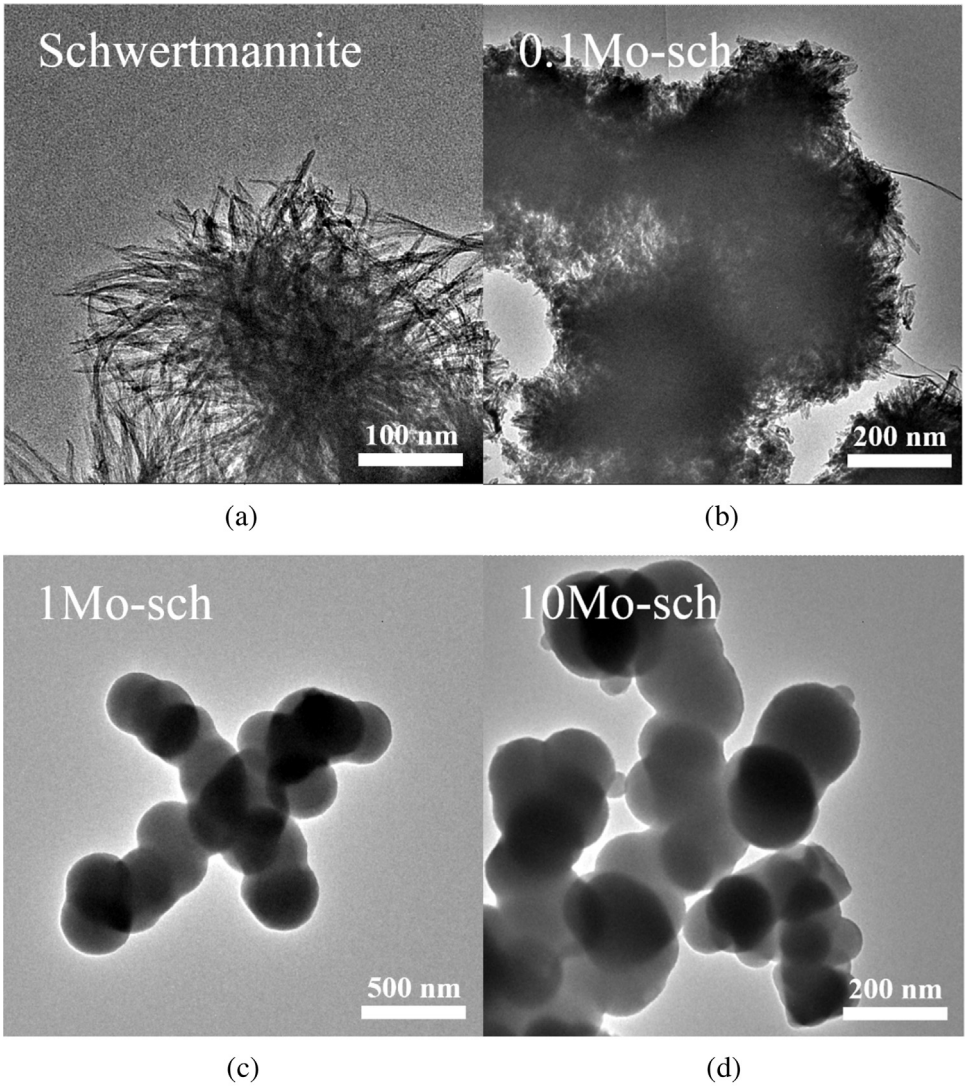

Fig. 2. TEM analyses of Sch after MoO_4^{2-} immobilization at initial pH 3.0 after 24 h with a initial MoO_4^{2-} concentrations of (a) 0 mM and (b) 0.1 mM, (c) 1.0 mM, (d) 10 mM. Initial concentration and of Sch was 1 g L^{-1} with a working volume of 150 mL.

ies also indicated that the incorporated arsenate in Sch stabilized the structure of Sch [24]. Given the similar radii and charges of molybdate and arsenate (SI Table 1), molybdate can also enter the structure of Sch and stabilize its crystalline structure. In addition, the new peak around 20° (Fig. 1) represents some characteristic peaks of $Fe_2(MoO_4)_3$ [25,26] merging with a hump of Sch. Deconvolution of the hump peak further indicates the presence of some characteristic peaks of $Fe_2(MoO_4)_3$ (SI Fig. 1), suggesting that a fraction of high concentrated Mo_{imm} reacts with Fe(III) on the surface of Sch and forms $Fe_2(MoO_4)_3$. The morphology of Sch also shows dramatic changes with increasing Mo_{imm} loadings. Compared with the cactus-like morphology of Sch, the needle particles on Sch degenerate with an increasing Mo_{imm} loading, and the Mo-Sch morphology changes to a collapsed cactus shape in 0.1Mo-Fe (Fig. 2b) and to a globular shape in 1Mo-Sch and 10Mo-Sch (Fig. 2c and 2d). FTIR spectrum further indicates that Mo_{imm} results in significant variations of ν_{SO} in Sch, and ν_3, ν_1 and ν_4 bands gradually degenerate with increasing Mo_{imm} loadings (Fig. 3). This is due to the exchange of MoO_4^{2-} with adsorbed or structural SO_4^{2-} in Sch, given similar ionic radii and charges of these two anions (SI Table 1) [18], The broad peak in the range of 700–900 cm^{-1}, assigned to a tetrahedric Mo species in $Fe_2(MoO_4)_3$, further confirms the presence of $Fe_2(MoO_4)_3$ on the surface of Mo-Sch (Fig. 3) [25].

3.2. Catalytic activity of Mo-Sch in phenol oxidation

Adsorption capacities of Sch to molybdate at pH 3.0 are in a range from 0.05 to 2.57 mmol Mo g^{-1} Sch as initial concentrations of molybdate changed from 0.05 to 10 mM (SI Table 2). The high adsorption capacities to molybdate can be explained by a special mechanism that 60% molybdate adsorbs on Sch via anion exchange and 40% via surface complexation [17].

Mo_{imm} shows an inhibitory effect on phenol oxidation, with only 61.55% phenol oxidized by H_2O_2 after 20 h in the presence of 1Mo-Sch (SI Fig. 2). However, such an inhibitory effect is not significant as to the adsorbed chromate and arsenate on Sch (SI Fig. 2). To further investigate the influence of Mo_{imm} on phenol oxidation, different Mo_{imm} loadings on Sch were tested. It is interesting to notice that catalytic activity in phenol oxidation is not always inverse proportional to the Mo_{imm} loading on Sch, and 0.1Mo-Sch shows the lowest catalytic activity, with only 25.96% phenol removed after 20 h (Fig. 4).

pH is an important indicator that determines oxidation efficiency of Fenton-like reactions. Solution pH of Mo-Sch always increased during the oxidation processes (SI Fig. 3), which is quite different from our previous findings that pH decreased from 3.0 to 2.85 during phenol oxidation catalyzed by the pure Sch (SI Fig. 3)

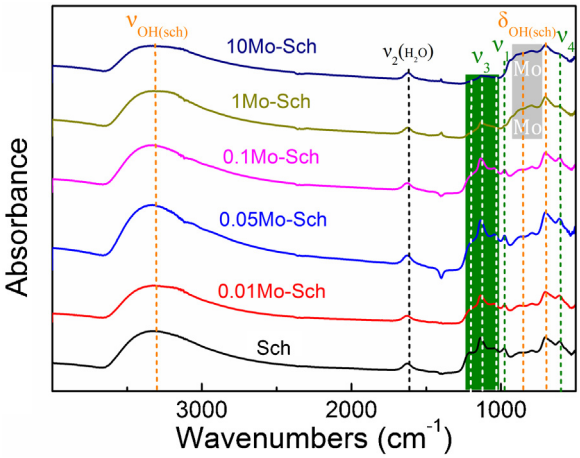

Fig. 3. FTIR spectra of freeze-dried Sch and Mo-Sch. Dominant vibrations include S—O stretches (ν_3, ν_1) and bend (ν_4), OH deformations of Sch ($\delta_{OH(sch)}$ at 860 and 712 cm^{-1}), and OH stretch of Sch ($\nu_{OH(sch)}$ at 3300 cm^{-1}).

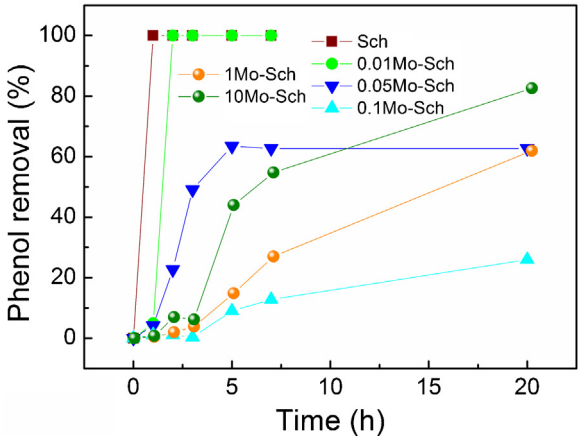

Fig. 4. Phenol oxidation by H_2O_2 catalyzed by Sch and Mo-Sch at initial pH 3.0 after 20 h. Initial concentrations of phenol, Sch and H_2O_2 were 100 mg L^{-1}, 1 g L^{-1} and 500 mg L^{-1}, respectively, with working volume of 150 mL.

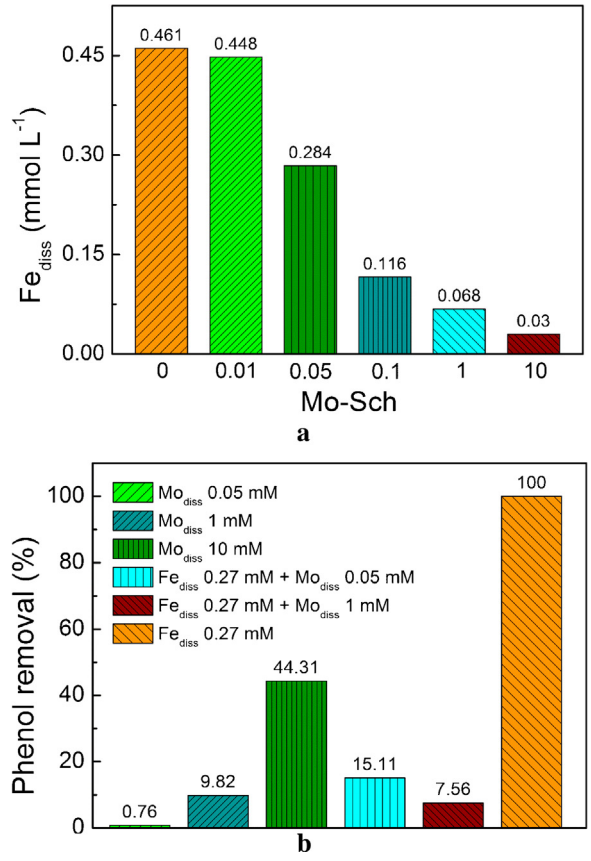

Fig. 5. (a) Iron dissolution from Sch during phenol oxidation at initial pH 3.0 after 20 h. Initial concentration of Sch was 1 g L^{-1} with a working volume of 150 mL; (b) Phenol oxidation by Fe_{diss} and/or Mo_{diss} in the absence of Sch at initial pH 3.0 after 20 h. Initial concentrations of phenol and H_2O_2 were 100 mg L^{-1} and 500 mg L^{-1}, respectively, with a working volume of 150 mL.

[4]. This indicates that oxidation mechanisms may be different in these two processes. In order to better understand correlations between phenol oxidation efficiency and the amount of Mo_{imm} on Sch, dissolved Fe(III) (Fe_{diss}) and Mo_{diss} released from Mo-Sch were measured.

3.3. *Catalytic activity of Fe_{diss} and Mo_{diss} in phenol oxidation*

Our recent study has confirmed the importance of Fe_{diss}, arising from Sch, in phenol oxidation by effectively catalyzing H_2O_2 to produce HO• radicals, and the efficiency of phenol oxidation increased with increasing Fe_{diss} concentrations [4]. The gradual decrease of Fe_{diss} from 0.461 to 0.03 mmol L^{-1} with increasing Mo_{imm} loadings from 0 to 10 mM indicates that Mo_{imm} significantly inhibits the release of Fe(III) from Sch (Fig. 5a). Other adsorbed oxyanions such as arsenate and chromate also contribute to Fe(III) retention on Sch, thus inhibiting its dissolution and transformation [18,27]. However, the released Fe_{diss} is not always proportional to the catalytic activity of Mo-Sch in that phenol oxidation is more significantly inhibited in 0.1Mo-Sch than that in 1Mo-Sch and 10Mo-Sch (Fig. 4, SI Table 2), although Fe_{diss} in 0.1Mo-Sch is larger than those in 1Mo-Sch and 10Mo-Sch (Fig. 5a).

Another interesting observation is that 30–40% of Mo_{imm} was released into solution in 1Mo-Sch and 10Mo-Sch systems (calculated from SI Table 2), implying that Mo_{diss} may also contribute to phenol oxidation. Control experiments were thus conducted to investigate contributions of Mo_{diss}, Fe_{diss} and dissolved Fe + Mo [$(Fe + Mo)_{diss}$] to phenol oxidation. In the absence of Fe_{diss}, phenol oxidation efficiency increased with increasing Mo_{diss} loadings, and 44.31% phenol was removed after 20 h in the presence of 10 mM Mo_{diss} (Fig. 5b), indicating that Mo_{diss} alone can effectively activate H_2O_2 under acidic conditions. However, as to 1Mo-Sch and 10Mo-Sch, the released Mo_{diss} are 0.398 and 0.807 mM, respectively as calculated from SI Table 2. Given that 1 mM Mo_{diss} only achieved 9.82% phenol removal (Fig. 5b) the, contribution of Mo_{diss} to phenol oxidation in these two systems is not predominant.

Compared with the high concentration of Mo_{diss} (10 mM), Fe_{diss} with a much lower concentration of 0.27 mM achieved a complete oxidation of 100 mg L^{-1} phenol after 20 h (Fig. 5b). However, the presence of Mo_{diss} significantly inhibited the catalytic activity of Fe_{diss}, with only 15.11% and 7.56% of phenol oxidized after 20 h as to 0.27 mM Fe_{diss} + 0.05 mM Mo_{diss} and 0.27 mM Fe_{diss} + 1.0 mM Mo_{diss} systems, respectively (Fig. 5b). This indicates that mechanism involved in phenol oxidation by Fe_{diss} is different from that by Mo_{diss}, and Mo_{diss} may interfere with the reactions between Fe_{diss} and H_2O_2. Given that concentrations of Fe_{diss} in 1Mo-Sch and 10Mo-Sch are also significantly smaller than 0.27 mM, the contribution of Mo_{diss} + Fe_{diss} to phenol oxidation in these two systems was insignificant.

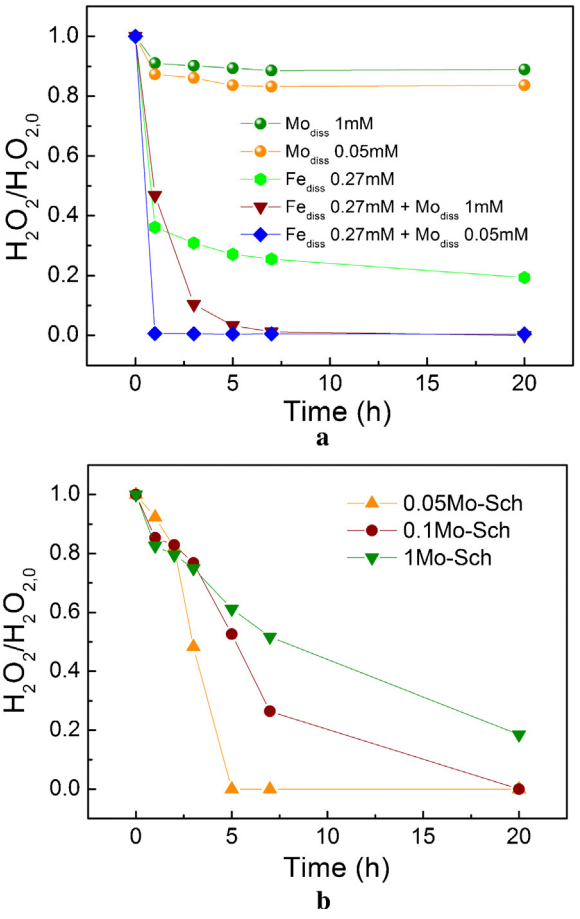

Fig. 6. (a) H_2O_2 decomposition by Fe_{diss} and/or Mo_{diss} in the absence of Sch at initial pH 3.0. Initial concentrations of phenol and H_2O_2 were 100 mg L^{-1} and 500 mg L^{-1}, respectively, with working volume of 150 mL; (b) H_2O_2 decompostion by Mo-Sch in phenol oxidation at initial pH 3.0. Initial concentrations of phenol, Mo-Sch and H_2O_2 were 100 mg L^{-1}, 1 g L^{-1} and 500 mg L^{-1}, respectively, with a working volume of 150 mL.

3.4. *Mechanisms of Mo_{diss} and Mo-Sch in phenol oxidation*

Decomposition rate of H_2O_2 is another important indicator to evaluate catalytic activity in Fenton-like reactions. Decomposition percentage of H_2O_2 was only 16.37% and 11.05% after 20 h as to 0.05 and 1 mM Mo_{diss}, respectively (Fig. 6a), implying that Mo_{diss} alone is not largely responsible for H_2O_2 decomposition. As Fe_{diss} and H_2O_2 coexist in solution, H_2O_2 is decomposed to HO• and •OOH radicals via Fenton-like pathways (Eqs. (2)–(4)). If Fe_{diss}, Mo_{diss} and H_2O_2 coexist in solution, decomposition rates of H_2O_2 are apparently accelerated (Fig. 6a). However, phenol oxidation efficiency is not significantly improved, with only 7.56% and 15.11% phenol oxidized in Fe_{diss}-1Mo_{diss}-H_2O_2-phenol and Fe_{diss}-0.05Mo_{diss}-H_2O_2-phenol systems, respectively (Fig. 5b). This implies that the rapid and complete decomposition of H_2O_2 does not necessarily generate oxidative radicals for phenol oxidation, because H_2O_2 can also be transformed into water and oxygen via a non-radical pathway [28]. Oxygen yield in the 0.27 mM Fe_{diss}-1Mo_{diss}-H_2O_2-phenol system further confirms that 88.32% H_2O_2 was rapidly transformed to O_2 after 5 h instead of reacting with phenol (SI Fig. 4). In comparison, 49.72% H_2O_2 was transformed to O_2 after 5 h in the 0.27 mM Fe_{diss}-H_2O_2-phenol system (SI Fig. 4), suggesting an accelerated decomposition rate of H_2O_2 in the coexistence of Fe_{diss} and Mo_{diss}.

On the other hand, since Fe_{diss} decreases with increasing Mo_{imm} loadings on Sch, H_2O_2 is more resistant to be decomposed as Mo_{imm} loadings change from 0.05Mo-Sch to 1Mo-Sch (Figs. 5a and 6b). As

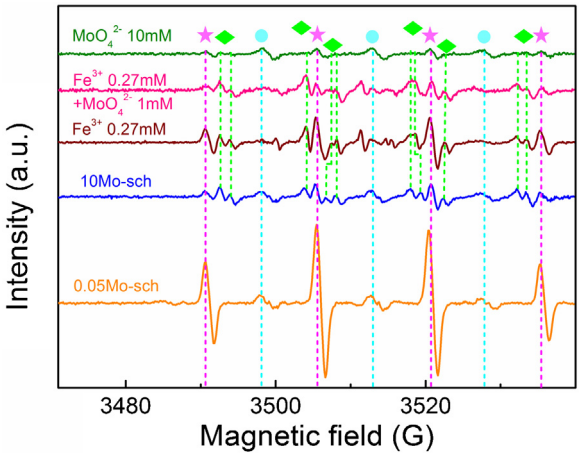

Fig. 7. EPR spectra in various systems of (a) 0.05Mo-Sch, (b) 10 Mo-Sch, (c) Fe_{diss} (0.27 mM), (d) Fe_{diss} (0.27 mM) + Mo_{diss} (1 mM) and (e) Mo_{diss} (10 mM) after 5 min (★, DMPO-HO•; ◆, DMPO-•OOH; ●, DMPOX). EPR conditions were 3515 G centerfield, 120 G sweep width, 9.85 GHz microwave frequency, 100 kHz modulation frequency, 10.03 mW power. Initial concentrations of phenol, heterogeneous catalysts and H_2O_2 were 100 mg L^{-1}, 1 g L^{-1} and 500 mg L^{-1}, respectively, with a working volume of 150 mL.

indicated in Fig. 6b, H_2O_2 was completely decomposed after 5 h and 20 h in 0.05Mo-Sch and 0.1Mo-Sch, respectively, whereas 19% H_2O_2 remained after 20 h in 1Mo-Sch.

Analyses of reactive radicals with EPR spectroscopy were carried out to examine possible radicals the generated in the Fe_{diss}, Mo_{diss} and Fe_{diss} + Mo_{diss} systems. EPR spectra show the typical DMPO-HO• adduct (the hyperfine splitting constants obtained by simulation, aN = 14.9 G, aH = 14.9 G, marked with asterisks), DMPO-•OOH adduct signals (aN = 14.2 G, aH = 11.3 G, and aH = 1.2 G, marked with rhombus), as well as the triplet signals of an unknown nitroxide, DMPOX (the oxidized product of DMPO, marked with round) (Fig. 7, SI Fig. 5 and 6) [29,30]. In the 0.27 mM Fe_{diss} system, EPR analysis confirms that H_2O_2 decomposition catalyzed by Fe(III) is a radical-chain reaction with the formation of HO• and •OOH radicals [31,32]. Once 1 mM Mo_{diss} is added into 0.27 mM Fe_{diss} solution, intensities of HO• and •OOH are significantly weakened, thus causing a significant decrease of phenol removal (7.56%), compared with that of 0.27 mM Fe_{diss} (100%) (Fig. 5b). This again confirms the interference of Mo_{diss} with the reaction between Fe_{diss} and H_2O_2, which effectively inhibits HO• generation. In addition, weak intensities of HO• and •OOH are also found in the 10 mM Mo_{diss} + H_2O_2 system, implying that these oxidative species are probably involved in phenol oxidation.

Given that $Mo_2O_3(O_2)_4^{2-}$ is a predominant Mo species formed from Mo_{diss} and H_2O_2 under acidic conditions [6], a visible variation of phenol-H_2O_2 mixture from colorless to yellow with an addition of 10 mM Mo_{diss} probably suggests the formation of $Mo_2O_3(O_2)_4^{2-}$ (SI Fig. 7). In order to further investigate whether this species can evolve the $^1O_2$, a species of which may contribute to phenol oxidation, 10 mM NaN_3, a strong $^1O_2$ scavenger [9,33] was added into the 10 mM Mo_{diss} + H_2O_2 + phenol mixture. Phenol oxidation efficiency was not significantly reduced after 20 h, ruling out the involvement of the $^1O_2$ in phenol oxidation at pH 3.0 (Fig. 8a). This is consistent with previous findings that $^1O_2$ generation was not favored as $Mo_2O_3(O_2)_4^{2-}$ dimer was predominant under acid conditions [9,34]. It is therefore deduced that $Mo_2O_3(O_2)_4^{2-}$ oxidized phenol directly via a non-$^1O_2$ pathway under acidic conditions.

Reactions involved in Fe_{diss}:

$$Fe^{3+} + H_2O_2 \rightarrow Fe^{2+} + H^+ + {}^{\bullet}OOH \quad (2)$$

$$Fe^{2+} + H_2O_2 \rightarrow Fe^{3+} + OH^- + HO^{\bullet} \quad (3)$$

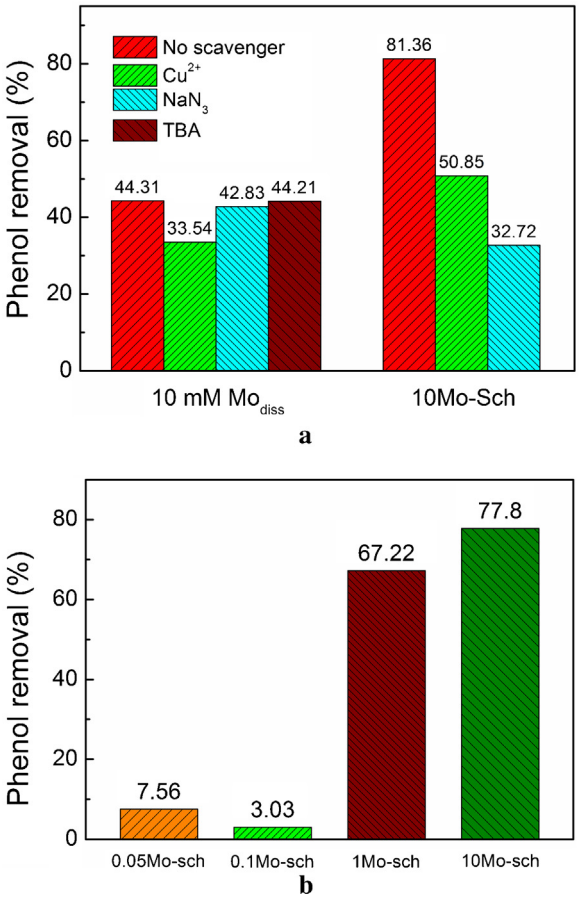

Fig. 8. (a) Addition of 5 mM Cu^{2+}, 5 mM NaN_3 or 200 mM *tert*-buthanol in 10 mM Mo_{diss} and 5 mM Cu^{2+} or 5 mM NaN_3 in 10Mo-Sch on phenol oxidation at initial pH 3.0 after 20 h. Initial concentrations of phenol, Mo_{diss}, 10Mo-Sch and H_2O_2 were 100 mg L^{-1}, 10 mM, 1 g L^{-1} and 500 mg L^{-1}, respectively, with a working volume of 150 mL. (b) Addition of 20 mM *tert*-buthanol in Mo-Sch systems on phenol oxidation at initial pH 3.0 after 20 h. Experimental conditions were the same as (a).

$$\bullet OOH + Fe^{3+} \rightarrow Fe^{2+} + H^+ + O_2 \quad (4)$$

Reactions involved in Mo_{diss}:

$$2H^+ + 2MoO_4^{2-} + 4H_2O_2 \rightarrow Mo_2O_3(O_2)_4^{2-} + 5H_2O \quad (5)$$

$$MoO_4^{2-} + nH_2O_2 \xrightarrow{OH^-} MoO_{4-n}(O_2)_n^{2-} + nH_2O (1 \le n \le 4) \quad (6)$$

$$Mo_2O_3(O_2)4^{2-} + nH_2O \xrightarrow{H^+} n\bullet OOH + n\,HO\bullet + Mo_2O_{3+n}(O_2)_{4-n}^{2-} (1 \le n \le 2) \quad (7)$$

$$Mo_2O_3\,(O_2)_4^{2-} + n\bullet OH \xrightarrow{H^+} n\,\bullet OOH + Mo_2O_{3+n}(O_2)_{4-n}^{2-} (1 \le n \le 4) \quad (8)$$

$$2MoO_{4-n}(O_2)_n^{2-} \xrightarrow{OH^-} {}^1O_2 + 2MoO_{6-n}(O_2)_{n-2}^{2-} (1 \le n \le 4) \quad (9)$$

Reactions involved in high Mo_{imm} on Sch:

$$\equiv MoO_4^{2-} + nH_2O_2 \xrightarrow{H^+} \equiv MoO_{4-n}(O_2)_n^{2-} + nH_2O (1 \le n \le 4) \quad (10)$$

$$\equiv MoO_{4-2n}(O_2)_{2n}^{2-} + nH_2O \xrightarrow{H^+} n\,\bullet OOH + nHO\bullet \equiv MoO_{6-2n}(O_2)2n - 2^{2-} (1 \le n \le 2) \quad (11)$$

$$\equiv MoO_{4-n}(O_2)_{n^{2-}} + \bullet OH \xrightarrow{H^+} \bullet OOH + \equiv MoO_{5-n}(O_2)_{n-1}{}^{2-} (1 \le n \le 4) \quad (12)$$

$$\equiv MoO_{4-n}\ (O_2)n^{2-} \xrightarrow{H^+} \equiv MoO_{6-n}(O_2)_{n-2}{}^{2-} + {}^1O_2 (1 \le n \le 4) \quad (13)$$

On the other hand, the presence of 5 mM Cu^{2+}, an effective scavenger to $O_2^{-}\bullet$/•OOH [35,36] reduced the phenol oxidation efficiency from 44.31% to 33.54%, suggesting that• OOH partially contributes to phenol oxidation (Fig. 8a). *tert*-butanol (TBA), a strong scavenger to HO• radicals [37], was also used to identify contribution of HO• radicals in the 10 mM Mo_{diss} + H_2O_2 + phenol system. Fig. 8a shows no inhibition of phenol oxidation in the presence of 200 mM TBA, suggesting that HO• radicals do not contribute to phenol oxidation. Although HO• has been detected in EPR analysis (Fig. 7, SI Fig. 6), its contribution to phenol oxidation is negligible due to its low concentration. In addition, it can be further transformed to OOH according to Eq. (8). Given the predominance of $Mo_2O_3(O_2)_4^{2-}$ under acidic conditions [6], ••OH and •OOH radicals should come from it (Eqs. (7) and (8)).

In Fe^{3+}-mediated Fenton reactions, •OOH and Fe^{2+} are formed in the reaction of Fe^{3+} and H_2O_2 (Eq. (2)), followed by H_2O_2 activation by Fe^{2+} and generation of •OH radicals (Eq. (3)). The side reaction between Fe^{3+} and •OOH consumes more H_2O_2 with the generation of O_2 (Eq. (4)). Given that $Mo_2O_3(O_2)_4^{2-}$ also provides •OOH radicals under acidic conditions (Eqs. (7) and (8)), such a reaction will accelerate Eq. (4) and produces more O_2 in the mixture of Fe_{diss}-Mo_{diss}-H_2O_2 (SI Fig. 4). Meanwhile, •OH radicals generated in Eqs. (3) and (7) can also react with $Mo_2O_3(O_2)_4^{2-}$ and provides more •OOH for O_2 production (Eqs. (4) and (8)).In order to differentiate whether HO• is a primary oxidant in phenol oxidation catalyzed by Mo-Sch, quenching experiments were conducted. In the presence of 20 mM TBA, less than 8% phenol was oxidized in 0.05Mo-Sch and 0.1Mo-Sch after 20 h (Fig. 8b), suggesting that at low Mo_{imm} loadings (0.01Mo-Sch or 0.05Mo-Sch), Mo-Sch is still able to catalyze H_2O_2 to produce HO• radicals by the released Fediss or the surface ≡Fe(III) [4]. On the other hand, 65% and 78% phenol can still be oxidized in 1Mo-Sch and 10Mo-Sch, respectively, and these values are comparable to 61.55% (1Mo-Sch) and 81.36% (10Mo-Sch) of phenol removal in the absence of TBA (Fig. 8b), suggesting that the primary oxidant in 1Mo-Sch and 10Mo-Sch systems are not HO•. EPR analysis further shows strong signal of HO• in the 0.05Mo-Sch system (Fig. 7), arising from H_2O_2 decomposition catalyzed by the released Fe_{diss} (0.284 mmol L^{-1}) (Fig. 5a) or the surface ≡Fe(III) on Sch. This agrees well with the quenching experiment that HO• plays a predominant role in phenol oxidation in the 0.05Mo-Sch system (Fig. 8b). However, high loadings of Mo_{imm} significantly inhibit the formation of HO• radicals, and low intensities of HO• and •OOH can be found in 10Mo-Sch (Fig. 7).

Unlike Mo_{diss}, Mo_{imm} on Sch prevents dimerization of molybdate with H_2O_2 and remains as a monomeric molybdate, which subsequently prevents the formation of $\equiv Mo_2O_3(O_2)_4^{2-}$ on Sch. On the other hand, this facilitates complexation between Mo_{imm} and H_2O_2 to form peroxo-Mo monomers such as $\equiv MoO_3(O_2)^{2-}$, $\equiv MoO_2(O_2)_2{}^{2-}$, $\equiv MoO(O_2)_3{}^{2-}$ and $\equiv Mo(O_2)_4{}^{2-}$ on Sch (Eq. (10)). The enhanced polarization of O—O and Mo—O_2 bonds in the immobilized peroxo-Mo monomers on the support facilitates H_2O_2 activation [38]. In order to make sure whether •OOH play a role in phenol oxidation, 5 mM Cu^{2+} was introduced into the 10Mo-Sch system. The decrease of phenol oxidation efficiency from 81.36% to 50.85% suggests a partial contribution of •OOH to phenol oxidation (Fig. 8a). Given that less HO• and more •OOH radicals are detected in 10Mo-Sch than those in 0.05Mo-Sch (Fig. 7), HO• in 10Mo-Sch is

assumed to activate $\equiv MoO_{4-n}(O_2)_n^{2-}$ and provides more •OOH for phenol oxidation (Eqs. (11) and (12)).

It is also interesting to notice that phenol oxidation efficiency decreased 49.34% in the presence of 5 mM NaN_3 in 10Mo-Sch + H_2O_2 system compared with that in the absence of NaN_3 (Fig. 8a), confirming the importance of $^1O_2$ in phenol oxidation in the 10Mo-Sch + H_2O_2 system. This is quite different from that in the Mo_{diss} system, in which nearly no contribution of $^1O_2$ to phenol oxidation was found. Although $^1O_2$ is usually generated from H_2O_2 catalyzed by Mo_{diss} under alkaline conditions (Eq. (1)), its generation has never been reported under acidic conditions. Mo_{imm} should be different from Mo_{diss} in H_2O_2 activation in that Mo monomers immobilized on Sch is more readily to complex with H_2O_2 and evolve $^1O_2$ (Eqs. (10) and (13)). We therefore believe that Mo speciation but not pH is necessary for $^1O_2$ evolvement. Previous study also suggested that the monomeric Mo in LDH-MoO_4^{2-} was necessary for $^1O_2$ generation [11], and dimeric molybdate did not favor $^1O_2$ generation [9,34].

On the basis of the above results, mechanisms involved in phenol oxidation catalyzed by Mo_{diss} and Mo-Sch are proposed. Under acidic conditions, $Mo_2O_3(O_2)_4^{2-}$, formed from molybdate and H_2O_2, can direct oxidize phenol via a non-$^1O_2$ pathway. •OOH, which is generated from $Mo_2O_3(O_2)_4^{2-}$, also partially contributes to phenol oxidation. As Fe_{diss} coexists with Mo_{diss}, Eq. (4) will be accelerated and more H_2O_2 will be more rapidly decomposed to O_2 via a non-radical pathway. Different from Mo_{diss}, mechanisms involved in phenol oxidation by Mo-Sch depend on Mo_{imm} loadings on Sch. At low Mo_{imm} loadings (0.01Mo-Sch and 0.05Mo-Sch), phenol oxidation is predominantly mediated by HO• radicals, whereas at high loadings (1Mo-Sch and 10Mo-Sch), •OOH radicals, generated from $MoO_{4-2n}(O_2)_{2n}^{2-}$ (Eqs. (11) and (12)), partially contribute to phenol oxidation. Different from Mo_{diss}, $^1O_2$ can be generated in the 10Mo-Sch + H_2O_2 system under acidic conditions, and plays an important role in phenol oxidation. The impossible dimerization between the immobilized molydate and H_2O_2 may facilitate complexation between Mo_{imm} and H_2O_2 and forms peroxo-Mo monomers of $\equiv MoO_{4-n}(O_2)_n^{2-}$ on Sch (Eq. (10)). Similar to $MoO_{4-n}(O_2)_n^{2-}$ under alkaline conditions, $\equiv MoO_{4-n}(O_2)_n^{2-}$ can also effectively activate H_2O_2 to generate $^1O_2$ radicals (Eq. (13)).

4. Conclusions

In this study, catalytic differences Mo_{diss} and Mo-Sch in the oxidation of phenol under acidic condition are illustrated. Dimeric $Mo_2O_3(O_2)_4^{2-}$, formed at pH 3.0 between molybdate and H_2O_2 can directly oxidize phenol via a non-$^1O_2$ pathway. •OOH, generated from $Mo_2O_3(O_2)_4^{2-}$ also partially contributes to phenol oxidation. Dimerization of Mo_{diss} with H_2O_2 inhibits $^1O_2$ generation. In Mo-Sch, mechanisms involved in phenol oxidation are dependent on the amount of Mo_{imm} on Sch. Phenol oxidation is predominantly mediated by HO• radicals at low Mo_{imm} loadings, whereas •OOH and $^1O_2$ play important roles at high Mo_{imm} loadings. We also find that Mo_{diss} interferes with the chain reactions between dissolved Fe(III) and H_2O_2, accelerating H_2O_2 decomposition via an O_2 generation pathway, which significantly reduces the utilization efficiency of H_2O_2 in phenol oxidation. This study enriches our understanding on the dual interference of molybdate on Fenon-like reactions catalyzed by iron (hydr) oxides or dissolved Fe(III). We also suggest that future work should be done to further illustrate $^1O_2$ generated pathways in Mo-Sch.

Acknowledgements

We greatly acknowledge the financial supports from the National Natural Science Foundation of China (XH, No. 41373114; No. 41201487) and the Natural Science Foundation of Tianjin (No. 15JCZDJC40200) (XH). We also thank technical supports of EPR analysis from Mr. Au Yu (Nankai University), and EPR analysis support from Prof. Ji-Hu Su (University of Science and Technology of China) and Ms. Jia-Hui Yang (Bruker Corporation).

Appendix A. Supplementary data

Supplementary data associated with this article can be found, in the online version, at http://dx.doi.org/10.1016/j.apcatb.2015.12.010.

References

[1] J.L. Wang, L.J. Xu, Crit. Rev. Environ. Sci. Technol. 42 (2012) 251–325.
[2] B.F. Sels, D.E. De Vos, P.A. Jacobs, J. Am. Chem. Soc. 129 (2007) 6916–6926.
[3] S. Sen Gupta, M. Stadler, C.A. Noser, A. Ghosh, B. Steinhoff, D. Lenoir, C.P. Horwitz, K.W. Schramm, T.J. Collins, Science 296 (2002) 326–328.
[4] W.M. Wang, J. Song, X. Han, J. Hazard. Mater. 262 (2013) 412–419.
[5] H.T. Duan, Y. Liu, X.H. Yin, J.F. Bai, J. Qi, Chem. Eng. J. 283 (2016) 873–879.
[6] N.J. Campbell, A.C. Dengel, C.J. Edwards, W.P. Griffith, J. Chem. Soc. Dalton Trans. 6 (1989) 1203–1208.
[7] V. Nardello, S. Bouttemy, J.M. Aubry, J. Mol. Catal. A: Chem. 117 (1997) 439–447.
[8] L.J. Csányi, J. Mol. Catal. A: Chem. 322 (2010) 1–6.
[9] B.F. Sels, D.E. De Vos, P.J. Grobet, F. Pierard, M.F. Kirsch-De, P.A. Jacobs, J. Phys. Chem. B 103 (1999) 11114–11123.
[10] J.M. Aubry, S. Bouttemy, J. Am. Chem. Soc. 119 (1997) 5286–5294.
[11] B.F. Sels, D.E. De Vos, P.A. Jacobs, J. Am. Chem. Soc. 129 (2007) 6916–6926.
[12] B.F. Sels, D.E. De Vos, P.J. Grobet, P.A. Jacobs, Chem. Eur. J. 7 (2001) 2547–2556.
[13] D.B. Yager, M.A. Mast, P.L. Verplanck, D.J. Bove, W.G. Wright, P.L. Hageman, Proceedings, 5th international conference on acid rock drainage, ICARD, 1 (2000) 535–547.
[14] J.R. Hayes, A.P. Grosvenor, J. Rowson, K. Hughes, R.A. Frey, J. Reid, Environ. Sci. Technol. 48 (2014) 4460–4467.
[15] Y. Arai, Environ. Sci. Technol. 44 (2010) 8491–8496.
[16] S. Goldberg, H. Forster, C. Godfrey, Soil Sci. Soc. Am. J. 60 (1996) 425–432.
[17] J. Antelo, S. Fiol, D. Gondar, R. López, F. Arce, J. Colloid Interface Sci. 386 (2012) 338–343.
[18] S. Regenspurg, S. Peiffer, Appl. Geochem. 20 (2005) 1226–1239.
[19] World Health Organization, Guidelines for Drinking-Water Quality, vol. 1, Recommendations, WHO, Geneva, 1984.
[20] EPA of China, Integrated Wastewater Discharge Standard (GB 8978-1996), State Environmental Protection Agency of China, Beijing, 1996.
[21] L. Clesceri, A. Greenberg, A. Eaton, Standard Methods for the Examination of Water and Wastewater, 20th ed., APHA, Washington, D.C, 2001.
[22] C. Vassilakis, A. Pantidou, E. Psillakis, N. Kalogerakis, D. Mantzavinos, Water Res. 38 (2004) 3110–3118.
[23] J.F. Boily, P.L. Gassman, T. Peretyazhko, J. Szanyi, J.M. Zachara, Environ. Sci. Technol. 44 (2010) 1185–1190.
[24] E.G. Garrido-Ramírez, B.K.G. Theng, M.L. Mora, Appl. Clay Sci. 47 (2010) 182–192.
[25] A.P.V. Soares, M.F. Portela, A. Kiennemann, L. Hilaire, J.M.M. Millet, Appl. Catal. A 206 (2001) 221–229.
[26] A.P.V. Soares, M.F. Portela, A. Kiennemann, Catal. Rev. 47 (2005) 125–174.
[27] E.D. Burton, S.G. Johnston, K. Watling, R.T. Bush, A.F. Keene, L.A. Sullivan, Environ. Sci. Technol. 44 (2010) 2016–2021.
[28] W.P. Kwan, B.M. Voelker, Environ. Sci. Technol. 36 (2002) 1467–1476.
[29] G.R. Buettner, M.K. Sharma, Free Radic. Res. 19 (1993) 227–230.
[30] L.L. Dugan, T.S. Lin, Y.Y. He, C.Y. Hsu, D.W. Choi, Free Radic. Res. 23 (1995) 27–32.
[31] B. Ensing, F. Buda, E.J. Baerends, J. Phys. Chem. A 107 (2003) 5722–5731.
[32] J.F. Perez-Benito, J. Phys. Chem. A 108 (2004) 4853–4858.
[33] M. Stylidi, D.I. Kondarides, X.E. Verykios, Appl. Catal. B: Environ. 47 (2004) 189–201.
[34] Q.J. Niu, C.S. Foote, Inorg. Chem. 31 (1992) 3472–3476.
[35] C.C. Chen, W.H. Ma, J.C. Zhao, Chem. Soc. Rev. 39 (2010) 4206–4219.
[36] O.S. Furman, A.L. Teel, R.J. Watts, Environ. Sci. Technol. 44 (2010) 6423–6428.
[37] I.S.X. Pinto, P.H.V.V. Pacheco, J.V. Coelho, E. Lorencon, J.D. Ardisson, J.D. Fabris, P.P. de Souza, K.W.H. Krambrock, L.C.A. Oliveira, M.C. Pereira, Appl. Catal. B: Environ. 119 (2012) 175–182.
[38] J. Wahlen, D.E. De Vos, B.F. Sels, V. Nardello, J.M. Aubry, P.L. Alsters, P.A. Jacobs, Appl. Catal. A 293 (2005) 120–128.